

NICMOS Status

Roelof S. de Jong, Santiago Arribas, Elizabeth Barker, Louis E. Bergeron, Ralph C. Bohlin, Daniela Calzetti, Ilana Dashevsky, Mark Dickinson, Anton M. Koekemoer, Sangeeta Malhotra, Bahram Mobasher, Keith S. Noll, Adam G. Riess, Alfred B. Schultz, Megan L. Sosey, Thomas Wheeler, Tommy Wiklind, Chun Xu

Space Telescope Science Institute, Baltimore, MD 21218

Abstract. We provide an overview of the most important calibration aspects of the NICMOS instrument on board of HST. We describe the performance of the instrument after the installation of the NICMOS Cooling System, and show that the behavior of the instrument has become very stable and predictable. We detail the improvements made to the NICMOS pipeline and outline plans for future developments. The derivation of the absolute photometric zero-point calibration is described in detail. Finally, we describe and quantify a newly discovered count-rate dependent non-linearity in the NICMOS cameras. This new non-linearity is distinctly different from the total count dependent non-linearity that is well known for near-infrared detectors. We show that the non-linearity has a power law behavior, with pixels with high count rates detecting slightly more flux than expected for a linear system, or vice versa, pixels with low count rate detecting slightly less than expected. The effect has a wavelength dependence with observations at the shortest wavelengths being the most affected (~ 0.05 - 0.1 mag per dex flux change at ~ 1 micron, 0.03 mag per dex at 1.6 micron).

1. Introduction

NICMOS is currently (December 2005) the second most used science instrument on board of the Hubble Space Telescope, accounting for about 25% of its science observations. NICMOS has been operating for more than 3.5 years with the NICMOS Cooling System (NCS) that was installed in March 2002 during Servicing Mission 3B. With the NCS the instrument is operating at a very stable temperature, making it easier to calibrate than in the pre-NCS period, as many instrument characteristics show a strong temperature dependence. NICMOS has become over the run of years a more mature instrument on HST with most of its characteristics well defined and corrected in the standard data reduction pipeline. However, in recent years NICMOS has been used at the extremes of its capabilities, revealing new, unexpected instrumental effects that we are in the process of calibrating. Examples of extreme use are grism observations of the $\sim 6^{\text{th}}$ H-mag exo-solar planet host star HD209458 (PI Gilliland, ID 9642) to the Hubble Ultra Deep Field with galaxies of about 24^{th} H-mag, a dynamic range of 18 magnitudes!

The organization of the paper is as follows. In section 2. we describe the main results of the different calibration programs, in general monitoring of the instrument under normal circumstances. In section 3. we describe developments of the NICMOS calibration pipeline and plans for future improvements. Section 4. gives a detailed account of the derivation of the photometric zero-point calibration. Investigations into the recently discovered count-rate dependent non-linearity are presented in section 5.. Our further calibration plans are described in section 6..

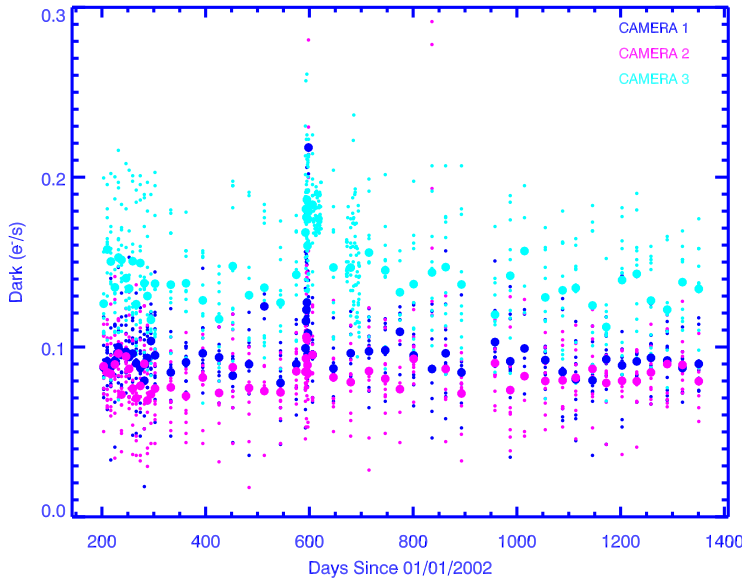


Figure 1.: Dark count rates in the three different NICMOS cameras.

More detailed information on many of the NICMOS calibration efforts are described in separate contributions to these proceedings.

2. Instrument

Several programs have been executed over the lifetime of NICMOS to monitor the behavior of key calibrations. One of the most important programs is the monitoring of the instrument temperature, as many instrument characteristic depend critical on temperature. We aim to keep the temperature as close as possible to 77.1 K, adjusting the cooling rate of the NCS if necessary to account for seasonal variations and other temperature drifts.

The dark count rate is monitored at regular intervals and has been found to be stable (Fig. 1). The high count rates in this figure seen near day 600 are due to persistence of Mars observations.

The focus of the three NICMOS cameras is monitored at regular intervals using phase retrieval (Fig. 2). No focus adjustments have been necessary since the installation of NCS. NIC1 and NIC2 are permanently in focus; NIC3 remains slightly out of focus due to dewar deformations developed before NCS installation which are outside the range of corrections possible with the NICMOS focussing mechanism. No special NIC3 focus campaigns shifting the HST secondary mirror are planned, as the NIC3 camera is significantly under-sampled and little is to be gained by such a dedicated campaign.

The count rates detected in the images of the flat field monitoring program have been very stable, indicating that there has been little change in sensitivity. However, the general shape of the flat field has been changing over time since NCS installation. The deviations are now about 1-3% from minimum to maximum in NIC1 and NIC3 (NIC2 is less affected) compared to the pipeline flat fields that were created after NCS installation. The effect is most severe at the shorter wavelengths. We are investigating whether these small flat field variations are the result of temperature changes using the temperature from bias method (Bergeron, these proceedings). New high signal-to-noise flat field observations are being planned.

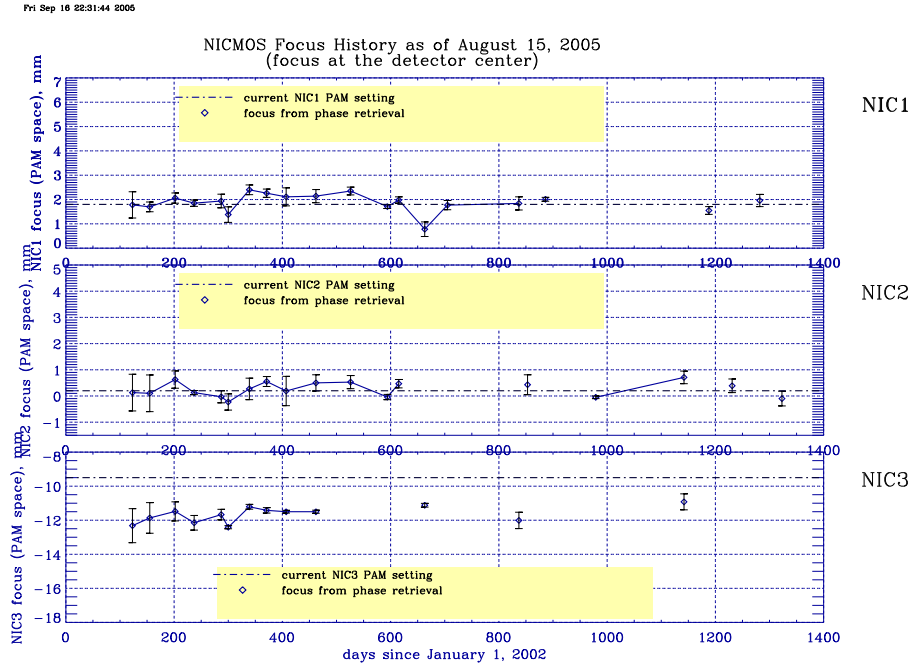


Figure 2.: Focus measurements of the three NICMOS cameras. NIC1 and NIC2 are at their nominal focus setting, NIC3 remains out of reach of the PAM focussing mechanism.

A number of programs were executed to investigate NICMOS performance in 2-gyro mode (see also Sembach, these proceedings). The NICMOS PSF shape did not change at the resolution of the NICMOS cameras as expected. Most critically, the coronagraphic rejection in the NIC2 camera did not suffer in 2-gyro mode. However, while the NICMOS coronagraphic mode is available, it is no longer possible to get two roll angle coronagraphic observation in one orbit due to the extra overhead involved in chancing guide stars under 2-gyro operations.

In June, 2005 new SPARS MULTIACCUM exposure time sequences (SAMP-SEQ) became operational, replacing the old MIF sequences. The new sequences are SPARS4, SPARS16, SPARS32 and SPARS128, complementing the already existing SPARS64 and SPARS256 sequences. These sequences have equal time steps between each readout. We recommend the use of these SPARS sequences for most observations, as they provide the most stable measurements especially in terms of amplifier glow. The alternative STEP sequences should only be used in situations where one needs to observe objects with a very large dynamic range in one observation.

Many of these (and other) calibration investigations have been described in Instrument Science Reports, which can be found at: <http://www.stsci.edu/hst/nicmos/documents/isrs>

3. Pipeline

Several enhancements are currently underway or have recently been implemented for NICMOS analysis routines and pipeline-related software. The MultiDrizzle software (Koeke-moer et al. 2002, 2005) available within Pyraf has been extended to enable fully automated combination of calibrated NICMOS images, which can be provided either as a list of exposures or as a NICMOS association table. We have also distributed the first Pyraf release of the "SAAclean" task (Barker et al. 2005) which is based on the IDL algorithm (Bergeron and Dickinson 2003) to remove residual flux from pixels impacted by cosmic rays accumulated during passage through the South Atlantic Anomaly. Testing is currently underway on

both MultiDrizzle and SAAclean to prepare them for eventual inclusion into the automatic processing carried out by the HST archive pipeline.

Development is also currently proceeding on a task to remove the cross-talk effect known as "Mr. Staypuft", where flux from bright sources on one quadrant can be seen to propagate to pixels in corresponding locations on the other quadrants. This task will be released to the community in an upcoming Pyraf release, and may eventually also be incorporated as part of the HST pipeline. Future work will include software to determine the NICMOS detector temperature from bias and voltage measurements, as well as improved amplifier glow and pedestal correction software which will most likely make use of the improved temperature measurements.

4. Photometry zero-point

Initial absolute photometric calibrations for NICMOS were obtained during SMOV in July 1997. These preliminary results used only a few filters in each camera to establish initial corrections from the predicted ground-based vacuum measurements. These measurements obtained accuracies between 10 and 15 percent. Later observations improved the calibration to about the 5% level in all cameras and filters by May 1998. However, revised ground-based photometry from Persson et al. 1998 suggested that calibrations based on the these CDBS (Calibration Data Base System) NICMOS photometric standard stars observations might be off by as much as 5 - 14 percent in some filters, due to an 0.1 magnitude discrepancy with the ground-based photometry for the solar analog and white dwarf used for calibration.

With the installation of the NCS the NICMOS detectors are operating at dramatically higher temperature with an associated strong change in sensitivity. Furthermore, the limited accuracy of previous analyses, new reduction routines, improvements to the pipeline calibrations and calibration images, and a better understanding of the instrument born anomalies encouraged a complete re-analysis of all available NICMOS photometric calibration data. The following paragraphs will discuss calculation of new aperture corrections for each camera/filter combination, improvements of the spectrophotometric standard star spectra used for calibration and an assessment of the overall photometric stability during the full lifetime of the instrument.

All standard star observations were reduced with the latest version of the calibration pipeline and reference files. In post-pipeline processing quadrant dependent bias was removed with *pedsky* and residual readout shading was removed by 1D fitting of the sky.

4.1. Aperture Corrections

Previous calibrations used a single aperture correction regardless of the filter element to correct the fixed aperture standard star photometry to an infinite aperture. While this can be used consistently for point source observations, the wavelength dependence of the PSF makes this incorrect for calibrating extended sources and makes comparisons with ground-based observations difficult. New, wavelength dependent, aperture corrections for each of the cameras have been calculated using the TinyTim PSF modeling software. Figure 3 shows the new aperture corrections compared to the previous fixed corrections. The new aperture corrections, along with the aperture sizes and sky annuli used, are tabulated on the NICMOS photometry web site.

4.2. Absolute Spectrophotometric Standards

The photometric calibration keywords are derived from the comparison of the measured NICMOS count rates for the standard star observations to the spectral flux density of the standard star averaged over the NICMOS bandpass. There are no ground-based spectrophotometric observations of standard stars with complete coverage over the NICMOS

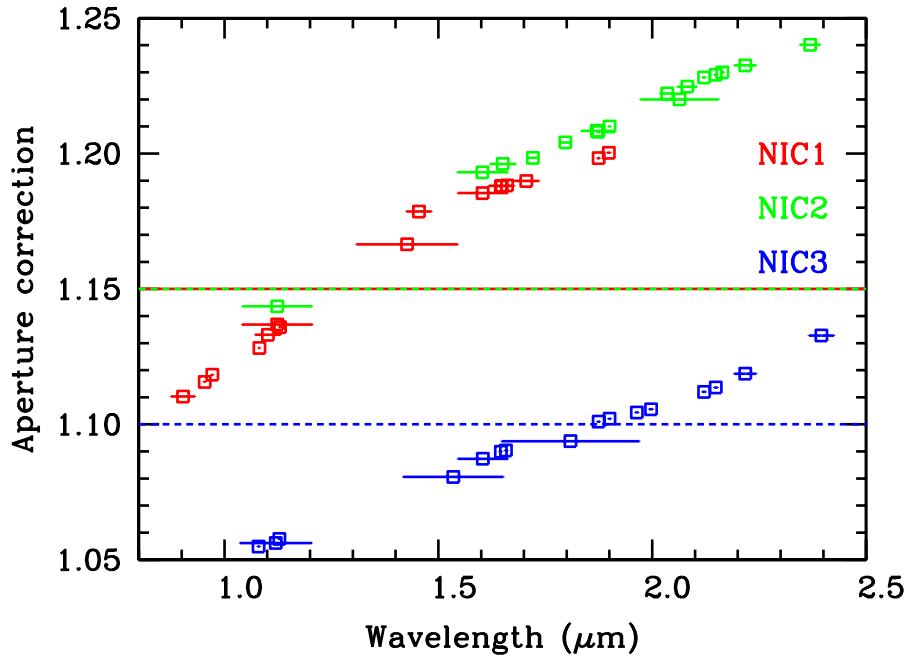


Figure 3.: Comparison of the old aperture corrections (dashed lines) with the new aperture corrections (squares, the filter widths are indicated by the horizontal line).

wavelength range, and therefore we must use accurately calibrated "surrogate spectra" instead in our comparison. This was the motivation for using solar analog and white dwarf standards for the NICMOS photometric calibration. The absolute spectral energy distribution of the Sun is well known (see Colina, Bohlin & Castelli 1996 and references therein), and thus can be scaled reliably to represent the spectrophotometry for solar analog standard stars like P330E. DA white dwarfs like G191B2B have relatively simple stellar atmospheres, and considerable effort has gone into accurately modeling these and comparing them to UV-through-optical spectrophotometry (Bohlin, Colina & Finley 1995; Bohlin 1996; Bohlin 2000).

As described by Colina & Bohlin 1997, the infrared spectrum of P330E is represented by the solar spectrum from Colina, Bohlin & Castelli 1996. The white dwarf G191B2B is represented by an LTE model calculated by D. Finley (described in Bohlin 2000). These spectrophotometric models are then normalized using ground-based photometry of the NICMOS standard stars. Persson et al. (1998) have obtained ground-based JHK photometry for a large set of faint infrared standard stars, including the HST/NICMOS solar analog standards. Persson (private communication) also observed G191B2B as part of the same program.

In order to normalize the standard star spectral models, we must convert Persson's JHK magnitudes to absolute flux density units. Campins, Rieke & Lebofsky (1985) provide an absolute infrared flux calibration scale using a solar analog method. However, the effective wavelengths and bandwidths of their JHK filters (which we will refer to as the Arizona system, where Vega is defined to have $J=H=K=0.02$) differ somewhat from those used by Persson et al. (calibrated to the CIT system, where Vega is defined to have $J=H=K=0.0$). In order to shift the Campins et al. absolute calibration to the Persson et al. bandpasses, we have used an ATLAS 9 atmosphere model for Vega. This model is not used for any absolute calibration, but simply to compute flux density ratios for Vega between the Arizona and Persson et al. bandpasses. These are then used to convert the Campins et al. Vega flux densities to the Persson et al. bandpasses, and hence to provide the absolute flux density

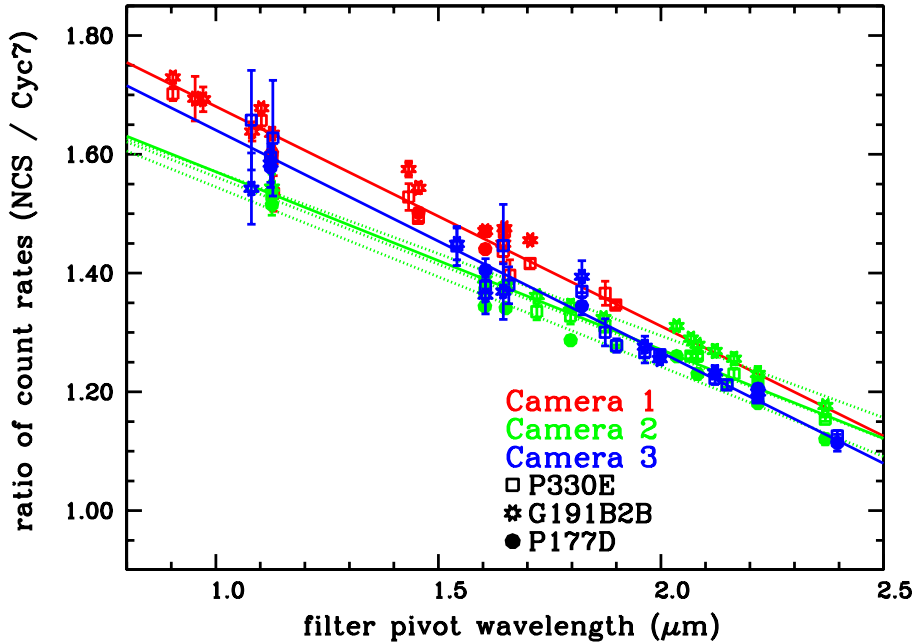


Figure 4.: The relative change in count rate of standard stars from Cycle 7 to post-NCS observations. The lines are linear fits to the data of the three cameras

calibration for the Persson et al. measurements. In this way, $m=0$ is calibrated to be 1626, 1056, and 658 Jy for the Persson et al. *JHK* bandpasses, respectively.

The P330E and G191B2B spectrophotometric models are then synthetically integrated through the Persson et al. *JHK* passbands, and the bandpass-averaged flux densities are converted to magnitudes for comparison to the ground-based photometry. This comparison indicates that the Colina & Bohlin (1997) P330E model requires an average flux re-normalization of +7% to match the *JHK* photometry at the 0.01 mag level. For G191B2B, the synthetic and ground-based photometry agree precisely (0.002 mag) at *J* and within 0.02 mags at *K*, but differ by 0.053 mags at *H*. We adopt the Bohlin (2000) G191B2B model without change, but note this possible discrepancy near 1.6 microns.

4.3. Zero-point Calibration

For each standard star we determined the average aperture count rate for all NIC1, NIC2, and NIC3 filters for each dither position and the many repeat observations. Observations near bad pixels or other outliers were removed from the average. The observed, aperture corrected, average total count rates for each star in each filter were compared with the predicted total count rates obtained using SYNPHOT synthetic photometry package¹ on the spectra of G191B2B and P330E. We used the *calcphot* program to calculate the effective stimulus of a source with a flat spectrum in f_ν . We used the ground-based filter shapes and detector quantum efficiency QE curve for the Cycle 7 data. The QE curve was modified for the post-NCS change in sensitivity by multiplying the QE with a linear correction that was determined from comparing pre-NCS to post-NCS count rates of standard stars (Fig. 4). Comparing the thus calculated effective stimulus to the observed average count rates results in the PHOTFNU keywords. Similar calculations provide the PHOTFLAM, PHOTPLAM and PHOTBW values found in NICMOS image headers, as described in the

¹available at http://www.stsci.edu/resources/software_hardware/stsdas/synphot

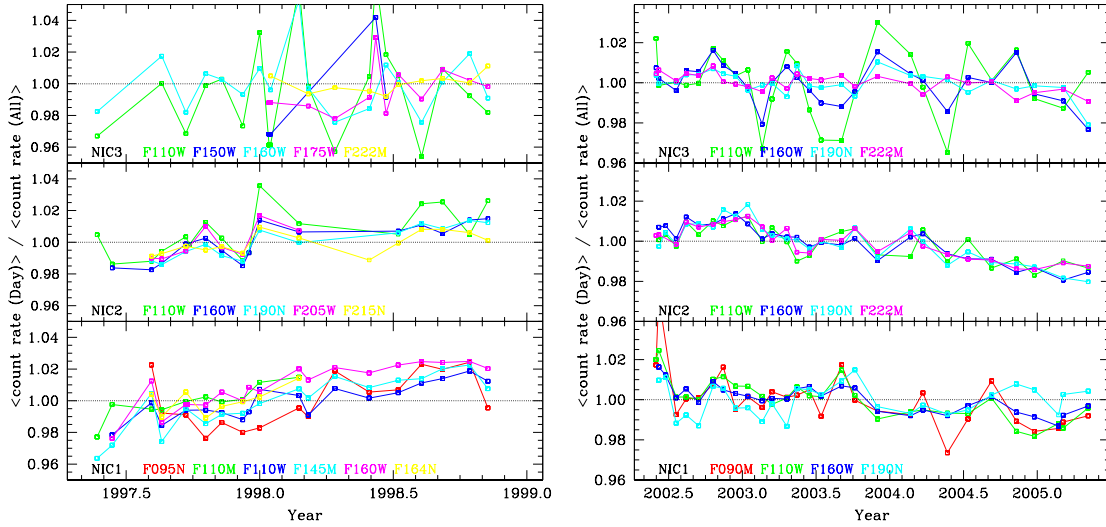


Figure 5.: Evolution of the P330E standard star count rates with left the Cycle 7 data and right the post-NCS data.

SYNPHOT manual and in Sirianni et al. (2005). The new calibration values have been automatically provided in the image headers retrieved from the HST archive since June 2004. The new filter throughput files were made available in the CDBS in December 2005. The latest calibration values can also be found at the NICMOS photometry web pages: <http://www.stsci.edu/hst/nicmos/performance/photometry>.

4.4. Photometric Stability

Photometric stability of NICMOS was investigated using all observations of Solar analog star P330E used in the photometric monitoring program (Fig. 5). The Cycle 7 data show the clear increase in sensitivity due to the increase in temperature while the solid nitrogen evaporated. After temperature correction there is a slight decrease in sensitivity. The post-NCS data show clear decrease in sensitivity in NIC2, a downward trend in NIC1, but the NIC3 data is too noisy due to intra-pixel sensitivity variations to tell whether there is any downward trend. The cause of this decrease in standard star sensitivity is not clear yet, as it is not matched in the flat field lamp monitoring data. However, similar downward trends are seen in the few repeat observations of G191B2B.

5. Non-linearity

In a recent analysis of NICMOS, STIS and ACS spectral data Bohlin et al. (2005) found that NICMOS shows a systematic count rate dependent non-linearity, primarily at the shorter wavelengths (Fig. 6). The same spectra show a similar non-linearity when compared to ACS photometry. This count-rate dependent non-linearity is distinctly different from the normal non-linearity of near-infrared detectors that depends on the total counts, not on the count rate. The total count non-linearity is well understood and corrected in the NICMOS pipeline.

The non-linearity is such that at high count rate there are more counts than expected, at low count rates less than expected, compared to intermediate count rates. The non-linearity shows no sign of turnover over the full 4 orders of magnitude measured (Fig. 6), and hence we cannot say with confidence that we are missing photon detections at the faint

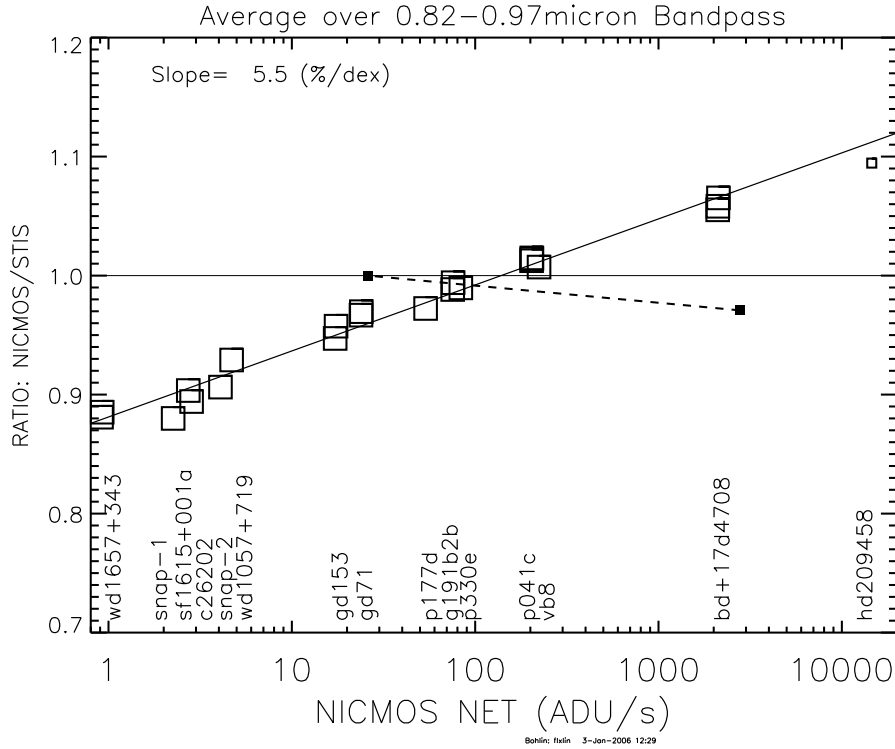


Figure 6.: Ratio of NICMOS grism fluxes to the STIS measurements averaged over the $0.82\text{--}0.97\mu\text{m}$ overlap range, normalized to the P330E ratio (big open squares) and least square fit (solid line). There is a non-linearity of about 5.5% per dex or a total of 23% over the 4 dex dynamic range in observed response. The bright star HD209458 was observed with NICMOS in a defocused mode and not included in the fit. Small filled squares connected by a dashed line—ACS grism fluxes compared to STIS in the same $0.82\text{--}0.97\mu\text{m}$ band. Over a dynamic range of $\sim 100\times$ between GD153 and BD+174708, the CCD detectors on STIS and the HRC in ACS measure the same relative flux to within 2%.

end or are getting extra detections at the bright end. The non-linearity is well modeled by a power law.

The count rates of the NICMOS spectra show in general good agreement with the NICMOS photometry count rates of the same objects, indicating that the NICMOS system is internally consistent and that it is not the spectral data reduction that is at fault. A few more indications have been found that NICMOS suffers from a non-linearity dependent on the incoming flux: 1) narrowband filters at the shorter wavelengths required larger in flight corrections from their ground-based determined throughputs than the broadband filters, 2) high redshift supernova fluxes are slightly fainter in F110W than expected based on their ACS fluxes and well tested SN models (Adam Riess, private communication), and 3) galaxies in the HUDF are slightly fainter than expected based on ACS and ground-based J&K magnitudes combined with SED modeling (Mobasher & Riess 2005; Coe et al., these proceedings).

However, all these lines of evidence rely on modeling of filter throughputs and/or spectral modeling of sources. Here we describe a test that depends on the change in incoming flux on the detector alone. NICMOS is a shutterless instrument and observes the sky while obtaining calibration flat fields using its internal lamps. The same object can be observed with an artificially increased flux and the count rate for objects can be compared with and without extra lamplight. For a fully linear system adding a background flux should not

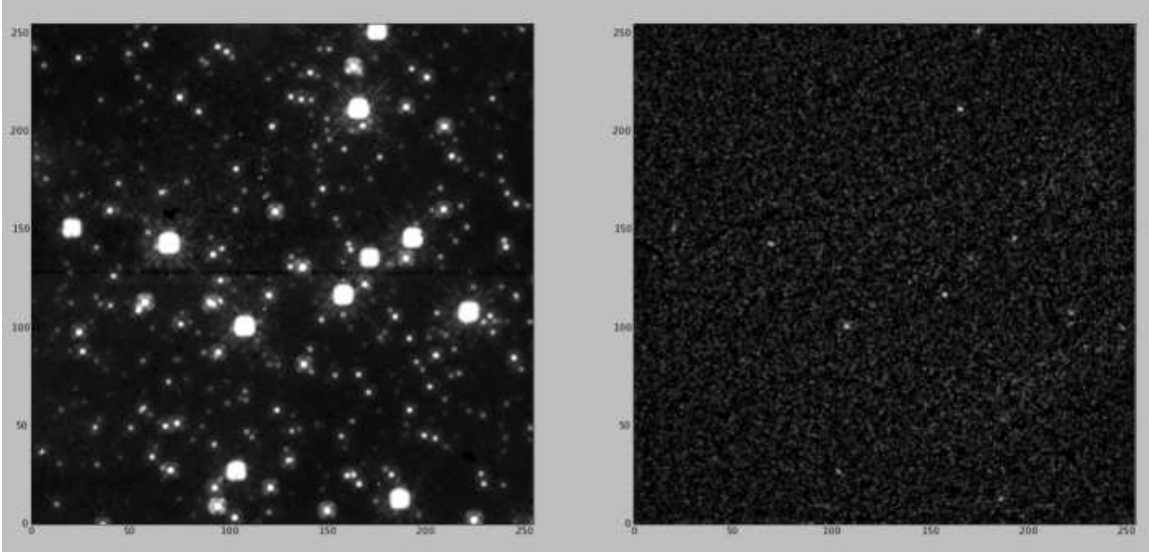


Figure 7.: (Left) NIC1 F110W lamp-off image of NGC 1850. (Right) NIC1 F110W lamp-on minus lamp-off image. Bright stars are clearly not well subtracted and leave residual flux as expected for count rate dependent non-linearity.

enhance the flux in the object, but any flux dependent non-linearity is revealed immediately when subtracting lamp-off images from lamp-on images.

Star cluster NGC 1850 was observed in the Cycle 14 calibration program in a sequence of lamp-off, lamp-on, and lamp-off using the same telescope pointing and without changing the exposure sequence. Similar observations taken in Cycle 7 for a different purpose were also analyzed. The data were analyzed under the assumption that a power law can model the non-linearity:

$$cr(x, y) \propto (f_{tot}(x, y))^\alpha,$$

with $cr(x, y)$ the measured count rate in ADU/s and $f_{tot}(x, y)$ the total flux falling on a detector pixel at (x, y) . For a non-linearity of $\sim 5\%$ per dex this corresponds to $\alpha \sim 1.02$. In magnitudes we have an offset of $\Delta m = 2.5(\alpha - 1)$ per dex change in incident flux. When we subtract the lamp-off from the lamp-on observation we expect to see positive residuals at positions where there are objects if $\alpha > 1$:

$$cr_{on} - cr_{off} \propto (f_{obj} + f_{sky} + f_{lamp})^\alpha - (f_{obj} + f_{sky})^\alpha \sim (f_{obj} + f_{lamp})^\alpha - (f_{obj})^\alpha,$$

where it is assumed that the sky flux is small compared to the other fluxes. Such image residuals are shown in Figure 7. The absolute boost in measured count rate is largest for bright objects, but the relative increase in measured count rate is larger for lower object fluxes, because the relative increase in flux by switching on the lamp is much larger. However, at low count rates the noise dramatically increases and we have to average many points to see the effect. This is shown in Figure 8, where we plot both the absolute and relative count rate increase due to the lamp background.

The fitted non-linearity functions are overplotted in Figure 8 and the measured α values are tabulated in Table 1. A number of points can immediately be taken from the Table. NICMOS has a significant count-rate dependent non-linearity, becoming more severe at shorter wavelengths. This is a different non-linearity from the well-known total count dependent non-linearity. The non-linearity in NIC1 and NIC2 amounts to 0.06-0.10 mag offset per dex change in incident flux for the shortest wavelength (F090M and F110W), about 0.03 mag/dex at F160W and less than that at longer wavelengths. These corrections are

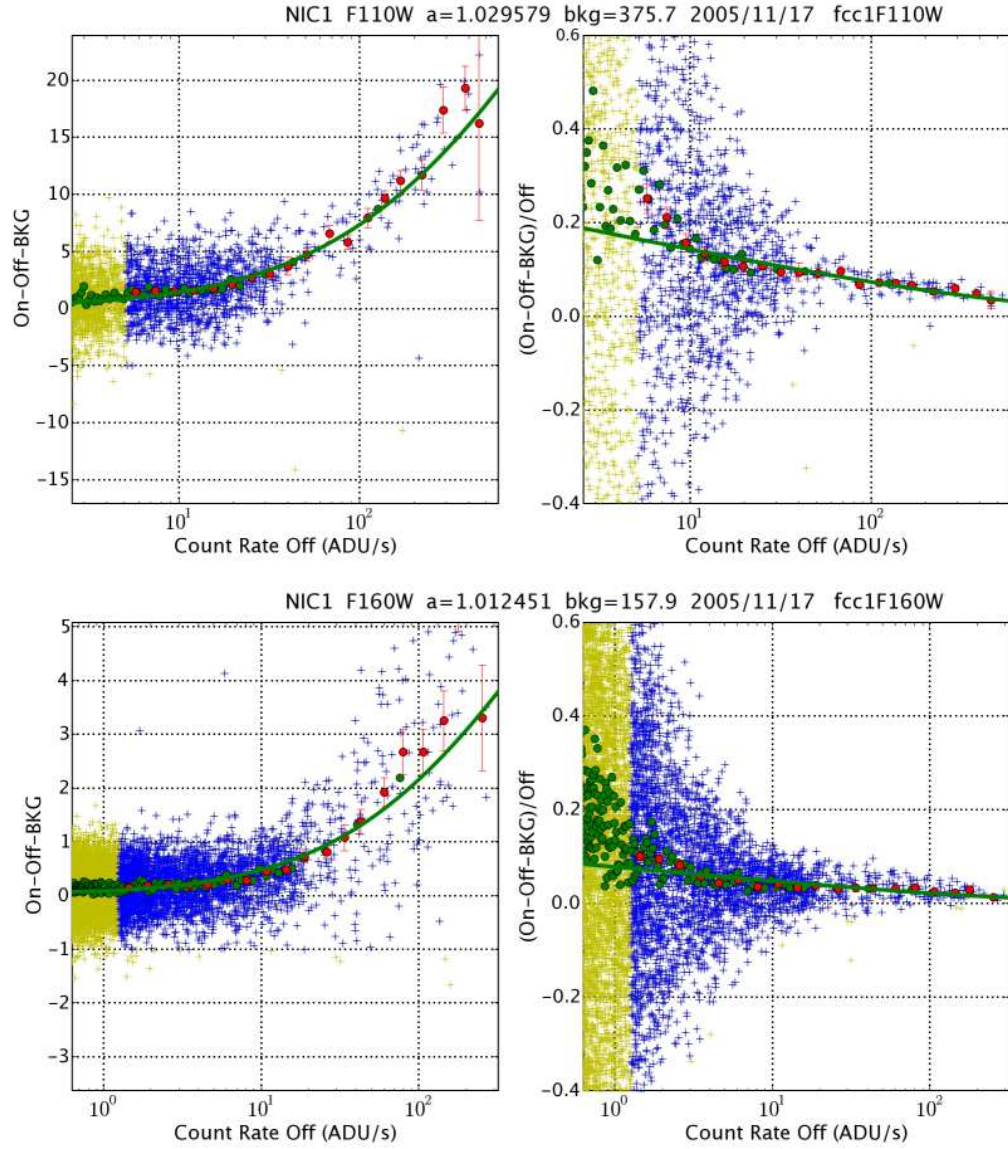


Figure 8.: The absolute and relative difference in lamp-on minus lamp-off count rates as function of the lamp-off count rates on a pixel-by-pixel basis. The yellow + symbols are for all data, the blue + symbols for the data used in the fit (bad and low S/N points filtered). The green circles are the averages in bins of 50 pixels in ascending lamp-off count rate for all pixels. The red circles are binned averages in 30 equal logarithmic steps in lamp-off count rate for the selected pixels. The green lines are the fitted non-linearity functions, with the fitted α parameter labeled at the top. Left is the absolute difference ($cr_{on} - cr_{off} - cr_{lamp}$), right is the relative difference $(cr_{on} - cr_{off} - cr_{lamp}) / cr_{off}$. While the brightest points have the largest flux change in absolute sense and are easy to measure above the noise (and are not due to background subtraction errors), the fainter points change relatively the most and have larger calibration errors relative to bright standard stars. Top) NIC1 camera, F110W filter. Bottom) NIC1, F160W filter.

Date	Camera	Filter	α	$\Delta m/\text{dex}$
Cycle 7				
1998/02/18	2	F110W	1.022 ± 0.001	0.055 ± 0.003
1998/04/17	2	F110W	1.025 ± 0.004	0.063 ± 0.010
1998/06/04	2	F110W	1.023 ± 0.001	0.059 ± 0.002
1998/08/06	2	F110W	1.024 ± 0.001	0.061 ± 0.002
1998/09/24	2	F110W	1.022 ± 0.001	0.054 ± 0.002
Cycle 14				
2005/11/17	1	F090M	1.040 ± 0.003	0.101 ± 0.008
2005/11/17	1	F110W	1.030 ± 0.003	0.074 ± 0.009
2005/11/17	1	F160W	1.012 ± 0.002	0.031 ± 0.006
2005/11/17	2	F110W	1.025 ± 0.002	0.063 ± 0.006
2005/11/17	2	F160W	1.012 ± 0.006	0.029 ± 0.015
2005/11/17	2	F187W	1.005 ± 0.004	0.013 ± 0.009

Table 1.: Measured α and Δm values in Cycle 7 and 14

larger than predicted from the Bohlin et al. (2005) NIC3 grism results, which may point to intrinsic detector differences or might be the result of a different analysis method. The non-linearity seems to have changed very little from Cycle 7 to Cycle 14 (in F110W NIC2), and hence is unlikely to depend on detector temperature. The fact that there is a wavelength dependence to the effect in the lamp off/on/off test and that this trend quantitatively agrees with the grism observations strongly argues against this being the result of a data reduction error and that the cause is intrinsic to the measurement.

To what extent NICMOS photometry is affected by the non-linearity depends on the wavelength of the observations (i.e. the α parameter), whether the object is a point source or extended, and on the count rate of the sky background (as the count rate will never go below the sky level and hence the non-linearity will level off, even if the sources have lower count rates). Given that the NICMOS standard stars are of about the 12th magnitude, the maximum expected offset for the Hubble UDF for example is about 0.15-0.2 mag at 22 F110W AB-mag, where the objects are comparable to or below the sky count level (see contribution by Mobasher, Thompson and Coe in these proceedings for further analysis of the HUDF).

The NICMOS team has as of yet not found a physical explanation for the count rate non-linearity. However, with these measurements we can start to calculate corrections to point source photometry. Software is being developed for more complicated cases with extended sources or objects close to the sky background level. Eventually corrections will be incorporated in the NICMOS calibration pipeline. Non-linearity lamp on/off calibration observations for all regularly used filter/camera combinations are currently being planned. More information on the NICMOS non-linearity and how to correct for it can be found at: <http://www.stsci.edu/hst/nicmos/performance/anomalies/nonlinearity.html>.

6. Calibration plans

The NICMOS team is currently implementing a calibration plan that addresses several of the anomalies observed above. New, high signal-to-noise flat field observations will be obtained for all filters regularly used. Dither observations with NIC1 have been obtained of star cluster NGC 1850 to investigate the low frequency flat field variations seen in the photometric monitoring data. Lamp on/off observations of star fields will be obtained in all regularly used camera/filter combinations to investigate the count-rate dependent

non-linearity. Details of the NICMOS calibration plan for Cycle 14 can be found in the contribution by Arribas to these proceedings.

References

- Barker, E. A., Koekemoer, A. M., Laidler, V. and Bergeron, E. 2005, HST Calibration Workshop (these proceedings)
- Bergeron, E. and Dickinson, M. 2003, NICMOS ISR 2003-010
- Bohlin, R. C. 1996, AJ, 111, 1743
- Bohlin, R. C. 2000, AJ, 120, 437
- Bohlin, R. C., Colina, L., & Finley, D. S. 1995, AJ, 110, 1316
- Bohlin, R. C., Lindler, D., Riess, A. 2005, NICMOS ISR-2005-002
- Campins, H., Rieke, G. H., Lebofsky, M. J. 1985, AJ 90, 896
- Colina, L., & Bohlin, R. 1997, AJ, 113, 1138
- Colina, L., & Rieke, M. J. 1997, 2003, in Proc. 2002 HST Calibration Workshop, ed. S. Arribas, A. Koekemoer, & B. Whitmore (Baltimore: STScI), 182
- Colina, L., Bohlin, R. C., & Castelli, F. 1996, AJ, 112, 307
- Koekemoer, A. M., Fruchter, A. S., Hook., R. N., & Hack, R. 2002, HST Calibration Workshop, 337
- Koekemoer, A. M., Fruchter, A. S., Hook., R. N., Hack, R., & Hanley, C. 2005, HST Calibration Workshop (these proceedings)
- Mobasher, M., & Riess, A. 2005, NICMOS ISR-2005-003
- Persson, S. E., Murphy, D. C., Krzeminski, W., Roth, M., & Rieke, M. J. 1998, AJ, 116, 2475
- Sirianni, M., et al. 2005, PASP, 117, 1049